

Ab-initio quantum transport through armchair graphene nanoribbons: streamlines in the current density

Jan Wilhelm,^{1,2} Michael Walz,^{1,2,3,*} and Ferdinand Evers^{1,2,3}

¹*Institute of Nanotechnology, Karlsruhe Institute of Technology, D-76021 Karlsruhe, Germany*

²*Institut für Theorie der Kondensierten Materie, Karlsruhe Institute of Technology, D-76128 Karlsruhe, Germany*

³*DFG Center for Functional Nanostructures, Karlsruhe Institute of Technology, D-76131 Karlsruhe, Germany*

(Dated: July 15, 2014)

We calculate the local current density in pristine armchair graphene nanoribbons (AGNRs) with varying width, N_C , employing a DFT-based ab-initio transport formalism. We observe very pronounced current patterns (“streamlines”) with threefold periodicity in N_C . They arise as a consequence of quantum confinement in transverse flow direction. Neighboring streamlines are separated by stripes of almost vanishing flow. As a consequence, the response of the current to functionalizing adsorbates is very sensitive to their placement: adsorbates located within the current filaments lead to strong backscattering while adsorbates placed in other regions have almost no impact at all.

PACS numbers: 72.80.Rj, 73.22.-f, 73.63.Nm

I. INTRODUCTION

The transmission has been investigated intensely in graphene nanoribbons (GNRs) experimentally^{1–8}, but also theoretically using tight-binding calculations^{9–15} and first-principles approaches^{16–23}. This strong interest in GNRs is closely related to their electronic properties: GNRs exhibit a bandgap^{24–26} that can be tuned with the ribbon width. This makes them promising materials for applications, e.g., in organic optoelectronics.

Quite generally, the design of functional devices will benefit from chemical modifications of pristine ribbons, for instance by placing adsorbates or substituents like boron or nitrogen to achieve *p*-type or *n*-type doping. The electrical conductance of functionalized armchair GNRs (AGNRs, see Fig. 1) is typically reduced due to resonant backscattering with localized states caused by the impurity^{10,11,16–19,22,23}. As is well confirmed by now, the impact of a single impurity on the conductance is extremely sensitive to its precise placing; the conductance can drop by an order of magnitude when shifting the adsorbate from one carbon atom to a neighboring one. Other defects, such as edge disorder^{9,13} or Stone-Wales defects^{12,13}, also affect the transmission but with a dramatically lower sensitivity to the precise defect location.

Motivated by this peculiar situation, we simulate in this paper the dc-current flow through pristine GNRs. Within tight-binding models, local (“bond”) currents are frequently discussed objects in the context of magnetism, e.g. in Ref. 27. Concerning experiments, first measurements of local dc transport properties have already been performed²⁸. In contrast, systematic theoretical investigations of local observables are still rare even for tight-binding models and almost absent on the ab-initio level.²⁹ In this context, it is important to notice that patterns in bond currents are difficult to interpret quantitatively — in particular with respect to the intensity of the current modulations. It is easy to see why: the standard tight-binding model describing the π electrons of conjugate carbon has only a single parameter that fixes the bandwidth. Without

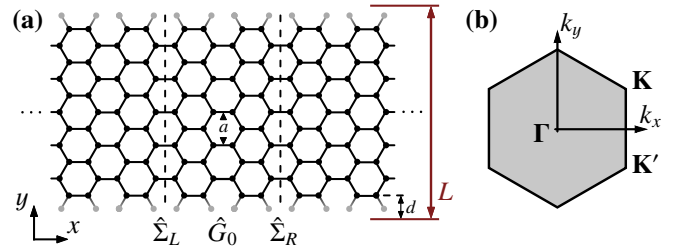


FIG. 1. (a) Structure of a hydrogen-terminated AGNR11 and (b) corresponding orientation of the Brillouin zone of the honeycomb lattice with the $\mathbf{K}/\mathbf{K}' = \frac{2\pi}{3a}(\sqrt{3}, \pm 1)$.

additional input, i.e., the explicit specification of real-space basis functions, a quantitative relation between bond currents and the physical current density cannot be established at all, strictly speaking.

For this reason, we set out in this work to investigate the general pattern of bias-induced current flows through GNRs quantitatively on the ab-initio level. A systematic dependency of the flow pattern on the ribbon width will be presented. The results will be interpreted as a manifestation of (transverse) quantum confinement. The reported sensitivity of the conductance of AGNRs to the precise placement of adsorbates will be explained and also why this sensitivity is absent in zigzag-nanotubes.

II. METHOD

In our calculations, we are employing the AITRANSS platform, our DFT-based transport simulation tool^{30–33}. The local current density is obtained as follows³⁴: We extract the Kohn-Sham (KS) Hamiltonian out of a DFT calculation for a structurally non-relaxed finite-size hydrogen-terminated graphene nanoribbon with horizontal armchair edges (see Fig. 1).³⁵ Subsequently, we obtain the (retarded) single particle KS-Green’s function \hat{G} of a finite-size strip in the presence of the

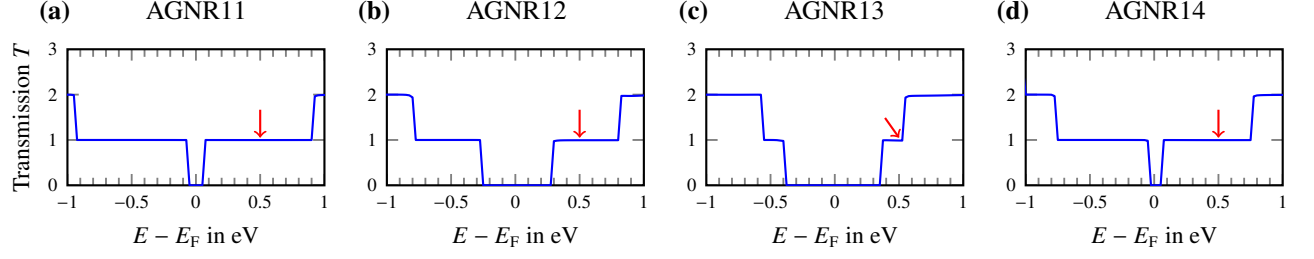


FIG. 2. Transmission of (a) AGNR11 to (d) AGNR14. The arrows indicate the current-patterns' energies in Fig. 3. The reference energy, E_F is the chemical potential of the isolated, charge-neutral species.

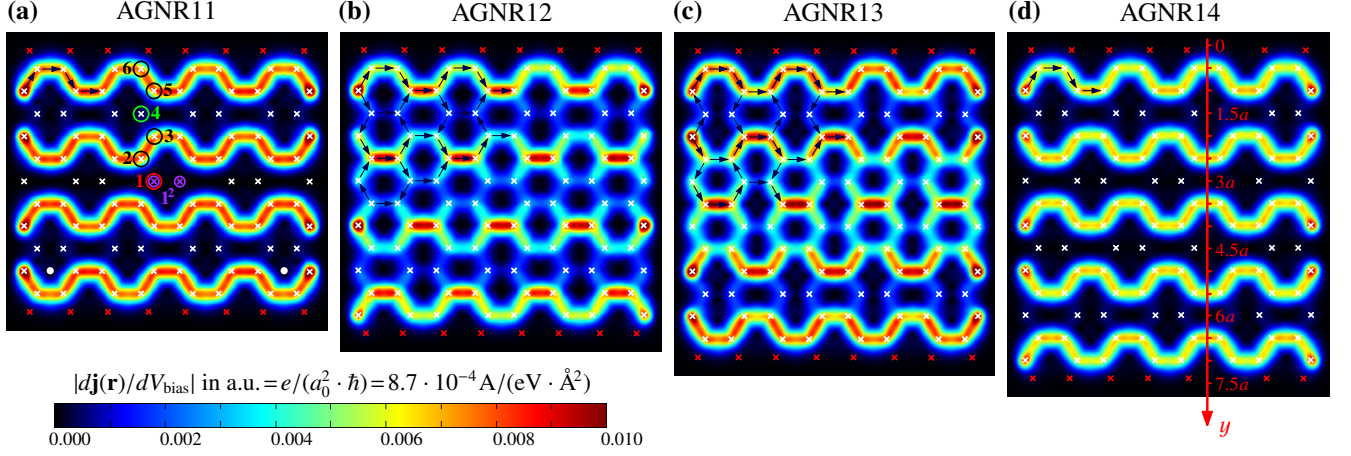


FIG. 3. Absolute value of the current density (per bias) associated with a fully transparent channel in a plane 0.5 \AA above the ribbon plane (exact energy $E = E_F + 0.5 \text{ eV}$, so $T(E) = 1$ for all ribbons, see Fig. 2). The current flows in horizontal direction as marked by the arrows. We checked that current patterns are identical for different energies E with $T(E) = 1$. The calculated transmission $T(E)$ is depicted in Fig. 2. Along the line in AGNR14, the current will be plotted for AGNRs($3m-1$) in Fig. 7.

left and right contacts by standard recursive Green's function techniques³⁶:

$$\hat{G}(E) = (\hat{G}_0^{-1} - \hat{\Sigma}_L - \hat{\Sigma}_R)^{-1}. \quad (1)$$

The self-energies $\hat{\Sigma}_R$ and $\hat{\Sigma}_L$ reflect the presence of the reservoirs³⁷, while \hat{G}_0 represents the bare KS-Green's function, see Fig. 1(a). The local currents follow from the non-equilibrium Green's function (NEGF) formalism. It features the lesser Green's function with $\hat{\Gamma}_\alpha = i(\hat{\Sigma}_\alpha - \hat{\Sigma}_\alpha^\dagger)$,

$$\hat{G}^<(E) = i\hat{G}(E)\hat{\Gamma}_L(E)\hat{G}^\dagger(E) \quad (2)$$

that relates to the local current density (per spin):

$$\left. \frac{d\mathbf{j}(\mathbf{r})}{dV_{\text{bias}}} \right|_E = \frac{1}{2\pi} \frac{\hbar^2}{2m} \lim_{\mathbf{r}' \rightarrow \mathbf{r}} (\nabla_{\mathbf{r}'} - \nabla_{\mathbf{r}}) G^<(\mathbf{r}, \mathbf{r}', E). \quad (3)$$

The factor $1/2\pi$ arises from an inverse Fourier transform.

III. RESULTS: TRANSMISSION AND CURRENT DENSITY

Fig. 2 displays the transmission function $T(E)$ of AGNRs of width N_C (Nomenclature: AGNR(N_C))³⁸. Here, $T(E)$ simply

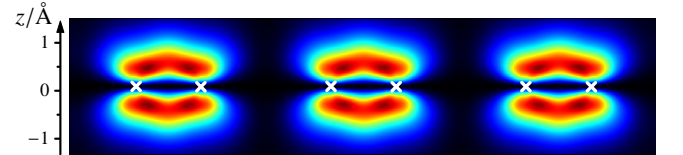


FIG. 4. Absolute value of the current density (per bias) in an AGNR11 at $T=1$ perpendicular to the ribbon plane between the white points out of Fig. 3(a) using the color scale of Fig. 3.

counts the energy bands intersecting with a given energy E . The bandgap characteristic of all AGNRs with its three-fold periodicity is clearly seen – minimum with AGNRs($3m-1$), $m \in \mathbb{N}$ ($\approx 0.1 \text{ eV}$). This observation reflects a well-known behaviour^{24-27,39}.

The corresponding current densities $d\mathbf{j}(\mathbf{r})/dV_{\text{bias}}$ are shown in Fig. 3 and Fig. 4. As one might expect, the current flows along chemical bonds following the π orbitals. Due to the central node of p_z orbitals, the current flow splits into an upper and lower sheet, see Fig. 4. Within the horizontal plane the current density $d\mathbf{j}(\mathbf{r})/dV_{\text{bias}}$ is strongly textured, see Fig. 3. For instance, in AGNRs($3m-1$) the current splits into m streamlines, with a fraction of horizontal bonds exhibiting zero flow. For these ribbons, the streamlines exist in a wide

energy window whenever there is a single transparent channel, $T(E)=1$. For other ribbons, AGNRs($\neq 3m-1$), streamlines survive at the edges, but start to mix in the bulk. Concerning their shape, the current patterns merely reflect the symmetry of the underlying molecular structure. AGNR11 and AGNR13 exhibit a horizontal symmetry axis in the middle, while the others exhibit a glide reflection symmetry.

Notice, that on the level of our simulations, we see no indication that this distinctive threefold periodicity in current patterns washes out at larger values of N_C .

IV. DISCUSSION: SELECTION RULES

In order to explain the current pattern, we invoke a standard zone-folding argument for graphene, here applied to AGNRs. Hard-wall boundary conditions in transverse current direction, y , imply a selection rule: $k_{y,n} = n\pi/L$, $n \in \mathbb{N}$. A natural choice is $L = (N_C + 1)a/2$ leading to

$$k_{y,n} = \frac{\pi}{(N_C + 1)a/2} \cdot n = \frac{2\pi}{3a} \cdot \frac{3n}{N_C + 1}, \quad (4)$$

with $a=2.46 \text{ \AA}$ being the graphene lattice constant.⁴⁰

For every ribbon with width N_C , there is a unique (see Fig. 5) integer \tilde{n} that minimizes the distance $|k_{y,n} - K_y|$, $K_y = \frac{2\pi}{3a}$. The implications of similar selection rules for the spectrum were already investigated and discussed by previous authors^{27,41,42}. Here, our interest is in the consequences for spatial properties, in particular the wavefunction's nodal structure and the node placing with respect to the carbon lattice. For this reason, we focus on the wavelength $\lambda_{N_C} = 2\pi/k_{y,\tilde{n}}$:

$$\lambda_{N_C} = 3a \cdot \begin{cases} 1 & \text{for } N_C = 3m - 1 \\ 1 + 1/N_C & \text{for } N_C = 3m \\ 1 - 1/(N_C + 2) & \text{for } N_C = 3m + 1 \end{cases}. \quad (5)$$

As can be seen from Fig. 6, the boundary conditions imply a partial mismatch of the wavefunction extrema with the carbon lattice. The exceptions are AGNRs($3m-1$), where the nodes of the wavefunction coincide with the carbon sites as a consequence of the perfect fit of $\lambda_0=3a$ into the box of width

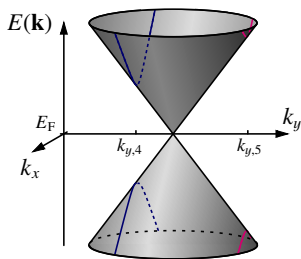


FIG. 5. Cone with discrete $k_{y,n}$ points near the Dirac point \mathbf{K} exemplary for an AGNR12. The states of this nanoribbon near the Fermi level are arranged on the hyperbolae with $k_{y,4} = 12/13 K_y$ and $k_{y,5} = 15/13 K_y$ due to Eq. (4). So, $k_{y,4}$ lies uniquely closest to the Dirac point, $\tilde{n}=4$.

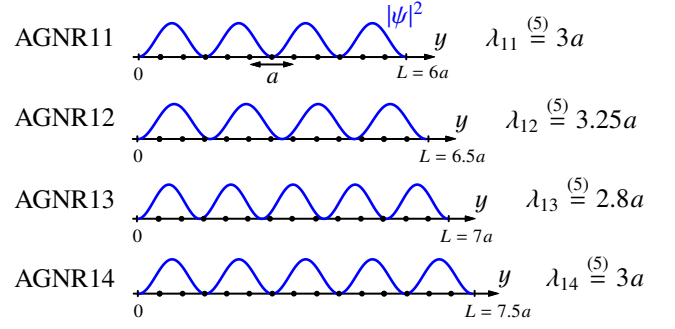


FIG. 6. Box with transversal density $|\psi|^2 \propto \sin^2(k_{y,\tilde{n}}y)$ of electronic states in a box with a wavelength according to Eq. (5). Charge carriers near the Fermi level have to jump to states with such an envelope when crossing an AGNR.

AGNRs($3m-1$). Hence, charge carriers have no probability amplitude on these carbon sites and therefore the connecting chemical bonds cannot carry current. Since there are $m-1$ disconnecting bonds, the number of streamlines is m . We recover the salient features of Fig. 3. Moreover, the simple particle-in-the-box picture predicts (i) that the shape of the current envelope is the same for each streamline and (ii) that the shape is independent of the ribbon width N_C . Both predictions are seen to be confirmed in Fig. 7.

The wavefunction's nodes of non-matching ribbons, $N_C \neq 3m-1$, are seen to be displaced from the carbon sites in Fig. 6, with small displacements near the edges and shifts of order of the lattice constant a in the bulk. Correspondingly, the current density shows streamlines near the edges but a less pronounced valley structure in the bulk, consistent with earlier observations in Fig. 3.

Further remarks: (a) All electronic states in a given band (e.g. see Fig. 5) exhibit the same k_y -component, i. e. share the same nodal structure. Therefore, they inherit the same current pattern which explains the robustness of the observed patterns, e.g., against shifting the Fermi energy. (b) If more than a single band contributes to the current, the total current will be a superposition of all bands with streamlines that in general

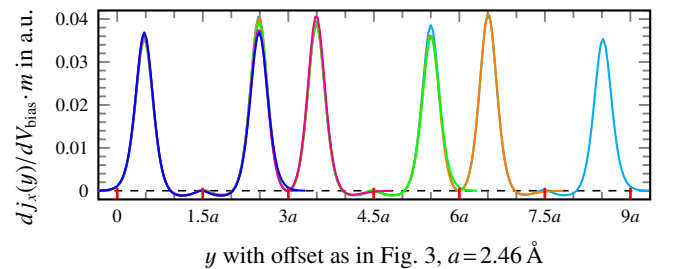


FIG. 7. x -component of the current density (per bias) scaled by the number of streamlines m at $E=E_F+0.5 \text{ eV}$ along the line sketched in the AGNR14 in Fig. 3(d) and analogously for AGNRs($3m-1$) with $N_C=5, 8, 11$ and 17 . Red ticks: node position, see Fig. 3 and 6. Negative currents near nodal lines indicate small current eddies with backflow.

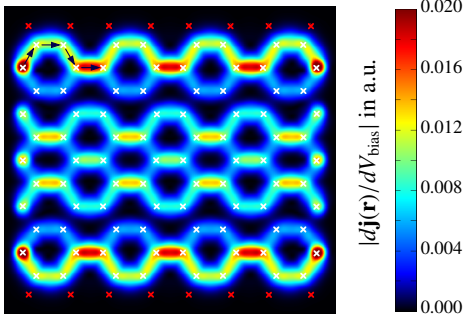


FIG. 8. Absolute value of the current density in an AGNR11 with two transmission channels, $T=2$ (again, in a plane 0.5 \AA above the ribbon, exact energy $E=E_F+1.0 \text{ eV}$). The observed pattern follows from a superposition of the channel at $T=1$ in Fig. 3 and an additional channel with a transversal wavelength $\lambda \neq 3a$. Similarly to AGNRs ($\neq 3m-1$) at $T=1$, streamlines survive at the edges, but start to mix in the bulk.

don't necessarily match. In this case, we observe a more complicated pattern, see the example in Fig. 8. (c) The energy interval ΔE with single-channel transport ($T(E)=1$) decreases with the ribbon width:

$$\Delta E = \frac{A}{N_C} \quad \text{with} \quad A = 25 \text{ eV}, \quad (6)$$

see Appendix A for more details. (d) The nodal structure of the wavefunctions is also displayed in the local density of states. Therefore, the nodal pattern may also be observed in STM experiments as simulations indicate⁴³, see Appendix B.

V. APPLICATION: ADSORBATE PLACING AND TRANSPORT

In the final section, we apply our results in order to explain earlier findings on the transport properties of functionalized AGNRs. It is well known^{16-19,22} that the impact of an impurity (adsorbate that promotes a carbon atom from sp^2 to sp^3 hybridization) on the transmission is very strongly site dependent. We confirm this observation in Fig. 9. It shows that the transmission function of an AGNR11 (structurally relaxed) in the presence of a single OH group is extremely sensitive to placement of the adsorbate. Shifting by one lattice site can change the transmission by orders of magnitude in a wide energy window.

When analyzing this observation in terms of streamlines, it has a very simple intuitive explanation. If streamlines don't touch the adsorption site (at pos. 1 and 4 in Fig. 3), the transmission is hardly affected by the OH group.⁴⁴ Our observation implies that even a finite concentration of adsorbates leaves the transmission invariant as long as they are placed in regions of zero flow (see Fig. 9 for the case of 2 OH). This allows an impurity concentration up to $1/3$ without significant influence on the transmission. By contrast, when placing an impurity right into a streamline (pos. 2, 3, 5 and 6 in Fig. 3), the transmission is strongly perturbed, see Fig. 9.

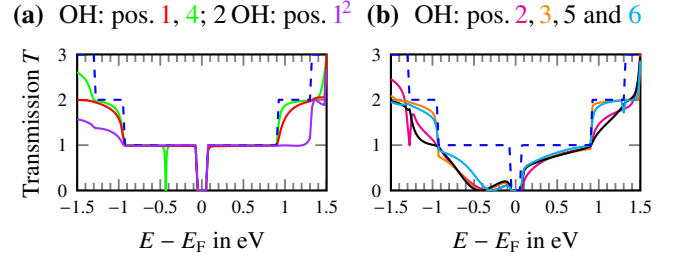


FIG. 9. Transmission of defected AGNR11 and the pristine case (dashed) for different OH positions out of Fig. 3. Left (right): OH is positioned outside (inside) a streamline.

Since the current pattern is a quantum confinement effect, one might wonder about the fate of the placing sensitivity after changing from hard-wall to periodic boundary conditions, i.e. from AGNRs to (zigzag) carbon nanotubes. Clearly, due to the transverse periodicity all carbon atoms are equivalent and therefore the tube's transmission cannot depend on the impurity placing, consistent with findings in the literature^{16,45}.

VI. CONCLUSIONS

In conclusion, we study the local current density per bias voltage, $d\mathbf{j}(\mathbf{r})/dV_{\text{bias}}$, in pristine armchair graphene nanoribbons with transport density functional theory. Our most important result is that $d\mathbf{j}(\mathbf{r})/dV_{\text{bias}}$ shows pronounced streamlines; the pattern exhibits a threefold periodicity in the width of the ribbon.

We explain the effect as a consequence of quantum confinement in transverse current direction. Due to streamlines, there is a strong sensitivity of the current response to the local placement of adsorbates. This sensitivity was well known before, and our results can provide an intuitive understanding of it. Finally, we mention that our results can also be understood as a manifestation of strong spatial structure in the scattering states of mesoscopic devices. We expect, that the structural elements — “current filaments” — that were observed in this study are a generic feature of transport through meso- and nano-devices that has hardly been touched upon by now.

ACKNOWLEDGMENTS

We thank C. Seiler and A. Bagrets for stimulating discussions and express our gratitude to the Simulation Lab NanoMicro, especially to I. Kondov, for computational support. The authors gratefully acknowledge the computing time granted by the John von Neumann Institute for Computing (NIC) and provided on the supercomputer JUROPA at Jülich Supercomputing Centre (JSC).

APPENDIX: ENERGY RANGE OF STREAMLINES AND STM IMAGES

In Appendix A, the energy interval where streamlines appear is discussed briefly. Appendix B provides simulation results for the energy-resolved equilibrium local electron density of AGNRs which can in principle be detected by a scanning tunneling microscope.

Appendix A: Energy window for observation of streamlines

As already mentioned in the body of the paper, the current pattern and the density pattern arrange in streamlines in AGNRs($3m-1$) only at energies E with a single, fully transparent channel. For energies farther away from the Fermi level, with two or more current channels, the patterns are more complicated. The energy range ΔE with $T(E)=1$ is equal to the distance between the second upper and the second lower band minus the bandgap, see Fig. 2 and Fig. 5. One expects a $1/N_C$ behaviour for this energy interval ΔE , since the discrete $k_{y,n}$ scale with $1/N_C$. This behaviour is checked in Table I for AGNRs($3m-1$).

We see a $1/N_C$ behaviour: The product of ΔE and N_C is approximately constant for bigger ribbons, while it is deviating strongly for smaller ribbons possibly caused by additional finite-size effects; Summarizing:

$$\Delta E = A \cdot \frac{1}{N_C} \quad \text{with} \quad A \approx 25 \text{ eV} \quad (\text{A1})$$

for AGNRs($3m-1$) with $m \geq 4$. In this energy interval, the streamlines with their characteristic nodes are expected to be detectable by STM. In particular, the energy window vanishes for the bulk limit $N_C \rightarrow \infty$.

Appendix B: STM images

1. Results: Local equilibrium density of states

The energy-resolved local equilibrium density of states (LDoS) in the presence of the leads is calculated as^{34,36}

$$\rho(\mathbf{r}, E) = -\frac{1}{\pi} \text{Im} G(\mathbf{r}, \mathbf{r}, E), \quad (\text{B1})$$

where $G(\mathbf{r}, \mathbf{r}, E) = \langle \mathbf{r} | \hat{G}(E) | \mathbf{r} \rangle$, see Eq. (1). The simulation results are shown in Fig. 10: The LDoS at 0.5 eV above the Fermi level shows strong texturing not only in the direction transverse to the current flow but also in longitudinal direction parallel to the streamlines (compare to Fig. 3). As one would expect, also the LDoS inherits the nodal structure of transverse wavefunctions near the Fermi level. For instance AGNR11 and AGNR14: the density on every third carbon atom (in transverse direction) vanishes consistent with Fig. 6.

Notice that in contrast to the density the current obeys the continuity equation, $\nabla \cdot \mathbf{j} = 0$. Hence, texturing in longitudinal direction is suppressed for the current resulting in streamlines that cannot be observed in the LDoS.

ribbon width N_C	Energy range ΔE with $T = 1$ in eV	$\Delta E \cdot N_C$ in eV
5	2.63 ^a	13.2
8	2.20 ^a	17.6
11	1.75 ^a	19.3
14	1.48 ^a	20.7
17	1.20 ^a	20.4
20	1.30 ¹⁶	26.0
35	0.75 ¹⁶	26.3
41	0.60 ^b	24.6
44	0.60 ¹⁸	26.4

TABLE I. Testing the dependency of ΔE and N_C for AGNRs($3m-1$). ΔE is defined as the energy range when only one band is present. All calculated values of ΔE are obtained by ab-initio calculations. In this energy interval ΔE , the streamlines appear. If the dependency $\Delta E(N_C)$ obeys an inverse correlation $\Delta E = A/N_C$, the product $\Delta E \cdot N_C$ will be A for all N_C . One shouldn't attach importance to the exact numerical values since they are strongly functional/method dependent.^a The ranges were extracted from transmission curves as in Fig. 2.

^b We applied the FHI-aims packages⁴⁶ using PBE functional for the DFT calculation employing tier1 basis set.

2. Pseudostreamlines in STM images at zero (in-plane) current flow

In the simplest picture (Tersoff-Hamann theory⁴⁷), a scanning tunneling microscope (STM) detects the energy-resolved local electron density of states (LDoS). Hence, the STM would detect patterns similar to Fig. 10 if it operated in a constant-height mode with a tip-distance z very close to the substrate: $z=0.5 \text{ \AA}$. With increasing the ribbon-tip distance, the STM resolves less and less features of the π -system so that the longitudinal texturing washes out, see Fig. 11. In contrast, the transverse nodal structure survives since even at large distances the sign change of the wavefunction can be detected. Therefore, one could expect that STM-images taken at larger distances show an LDoS patterned in a streamline-type manner ("Pseudostreamlines").

The simulated STM image out of Fig. 11 shows this feature. It is in perfect agreement with results of earlier authors⁴³, who have explained this pattern in a much more complicated way, though. They apply Clar's theory, a rule originating from organic chemistry^{48,49} that relies on a proper placing of (many) double bonds.

3. Experiments

We are not aware of experimental STM images of AGNRs($3m-1$) that would be showing streamlines or pseudostreamlines probably, because the control over the edge geometry is still an experimental challenge. Edges irregularities lead to electronic states with node structures strongly deviating from those of clean AGNRs($3m-1$).

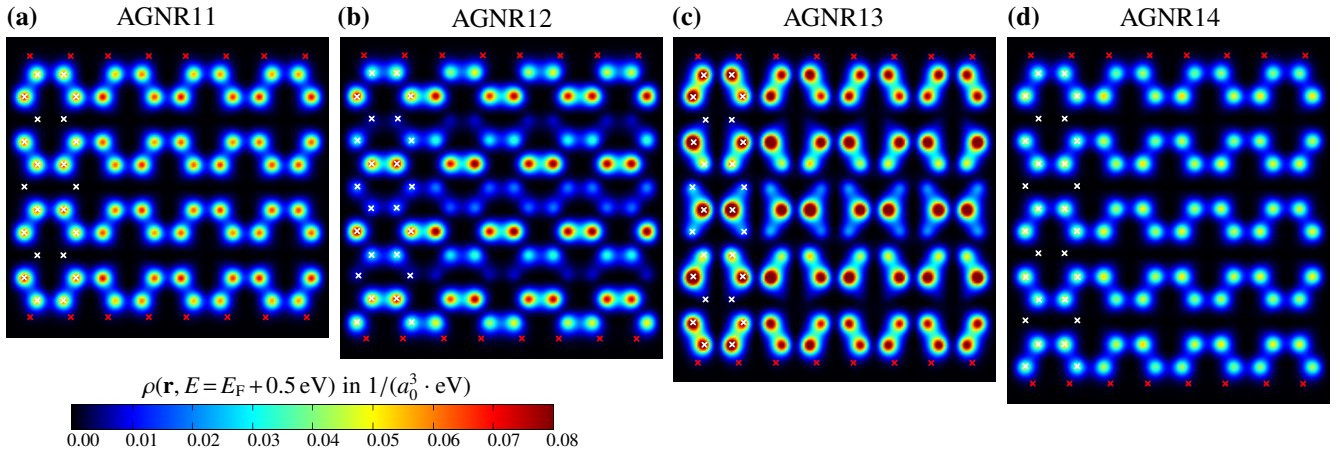


FIG. 10. LDoS in a plane 0.5 \AA above the ribbon plane (exact energy $E = E_F + 0.5 \text{ eV}$, so $T(E) = 1$ for all ribbons, see Fig. 2). We checked that the LDoS patterns are identical for energies E with $T(E) = 1$ except for their amplitude being dependent on the exact energy. Due to the close AGNR13's van Hove singularity (at $\approx E_F + 0.4 \text{ eV}$), the LDoS at $E = E_F + 0.5 \text{ eV}$ is enhanced in AGNR13 compared to the other AGNRs.

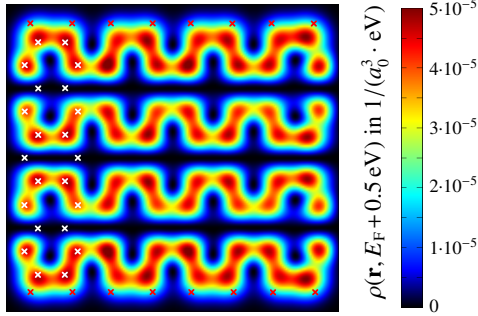


FIG. 11. LDoS of an AGNR11 in a plane 2 \AA above the ribbon plane at $E = E_F + 0.5 \text{ eV}$.

There are indications of the existing of standing wave patterns in other carbon based conjugate matter, namely in the fullerenes. Since also those may be thought of as graphene derivatives, one would expect a similar wavelength $\lambda = 3a = 7.4 \text{ \AA}$ to appear there as well.

Indeed, consider recent STM experiments on the fullerenes C_{58} and C_{60} .^{50,51} For a single fullerene, (low bias) STM images show an structureless circular spot, roughly consistent with the absence of the analogue of hard-wall boundary conditions — roughly similar to (zigzag) carbon nanotubes discussed above. Boundary conditions removing the rotational symmetry are realized with a formation of a chemical bond between two different fullerene cages. Then, STM images show a stripe pattern with a characteristic wavelength $\approx \lambda$. Given the discussion above, it is not surprising, perhaps, that this wavelength transfers from AGNR to fullerene electronic states near the Fermi level since fullerenes and nanoribbons are both a certain kind of derivate of graphene.

* michael.walz@kit.edu

- ¹ M. Y. Han, J. C. Brant, and P. Kim, Phys. Rev. Lett. **104**, 056801 (2010).
- ² L. Jiao, X. Wang, G. Diankov, H. Wang, and H. Dai, Nat. Nanotechnol. **5**, 321 (2010).
- ³ L. Liao, J. Bai, R. Cheng, Y. Lin, S. Jiang, Y. Huang, and X. Duan, Nano Lett. **10**, 1917 (2010).
- ⁴ A. Sinitskii, A. Dimiev, D. Kosynkin, and J. Tour, ACS Nano **4**, 5405 (2010).
- ⁵ F. Schwier, Nat. Nanotechnol. **5**, 487 (2010).
- ⁶ X. Wang, Y. Ouyang, L. Jiao, H. Wang, L. Xie, J. Wu, J. Guo, and H. Dai, Nat. Nanotechnol. **6**, 563 (2011).
- ⁷ A. Felten, B. S. Flavel, L. Britnell, A. Eckmann, P. Louette, J.-J. Pireaux, M. Hirtz, R. Krupke, and C. Casiraghi, Small **9**, 631 (2013).
- ⁸ A. Felten, A. Eckmann, J.-J. Pireaux, R. Krupke, and C. Casiraghi, Nanotechnology **24**, 355705 (2013).

- ⁹ T. C. Li and S. P. Lu, Phys. Rev. B **77**, 085408 (2008).
- ¹⁰ J. Y. Yan, P. Zhang, B. Sun, H. Z. Lu, Z. Wang, S. Duan, and X. G. Zhao, Phys. Rev. B **79**, 115403 (2009).
- ¹¹ S. Ihnatsenka and G. Kirczenow, Phys. Rev. B **83**, 245442 (2011).
- ¹² T. Lehmann, D. A. Ryndyk, and G. Cuniberti, Phys. Rev. B **88**, 125420 (2013).
- ¹³ S. Ihnatsenka and G. Kirczenow, Phys. Rev. B **88**, 125430 (2013).
- ¹⁴ A. Bergvall and T. Löfwander, Phys. Rev. B **87**, 205431 (2013).
- ¹⁵ A. Pieper, G. Schubert, G. Wellein, and H. Fehske, Phys. Rev. B **88**, 195409 (2013).
- ¹⁶ B. Biel, X. Blase, F. Triozon, and S. Roche, Phys. Rev. Lett. **102**, 096803 (2009).
- ¹⁷ A. Lopez-Bezanilla, F. Triozon, and S. Roche, Nano Letters **9**, 2537 (2009).
- ¹⁸ I. Deretzis, G. Fiori, G. Iannaccone, and A. La Magna, Phys. Rev. B **81**, 085427 (2010).
- ¹⁹ A. Cresti, A. Lopez-Bezanilla, P. Ordejón, and S. Roche, ACS

- Nano **5**, 9271 (2011).
- ²⁰ S. M.-M. Dubois, A. Lopez-Bezanilla, A. Cresti, F. Triozon, B. Biel, J.-C. Charlier, and S. Roche, ACS Nano **4**, 1971 (2010).
- ²¹ A. Lopez-Bezanilla and S. Roche, Phys. Rev. B **86**, 165420 (2012).
- ²² K. Saloriotta, A. Uppstu, A. Harju, and M. J. Puska, Phys. Rev. B **86**, 235417 (2012).
- ²³ M. Walz, J. Wilhelm, and F. Evers, (to be published).
- ²⁴ Y. W. Son, M. L. Cohen, and S. G. Louie, Phys. Rev. Lett. **97**, 216803 (2006).
- ²⁵ Z. F. Wang, Q. Li, H. Zheng, H. Ren, H. Su, Q. W. Shi, and J. Chen, Phys. Rev. B **75**, 113406 (2007).
- ²⁶ A. Dasgupta, S. Bera, F. Evers, and M. J. van Setten, Phys. Rev. B **85**, 125433 (2012).
- ²⁷ K. Wakabayashi, M. Fujita, H. Ajiki, and M. Sigrist, Phys. Rev. B **59**, 8271 (1999).
- ²⁸ As an example, the local electrical potential was measured by Kelvin probe force microscopy in graphene^{52–54}.
- ²⁹ A publication for GNRs, that we are aware of, employs a (nearest neighbor) tight-binding model to investigate a ribbon with $N_C=14$.¹⁰ Indeed, a pronounced pattern has been reported in the bond currents but a conclusive explanation has not been given.
- ³⁰ A. Arnold, F. Weigend, and F. Evers, J. Chem. Phys. **126**, 174101 (2007).
- ³¹ J. Wilhelm, M. Walz, M. Stendel, A. Bagrets, and F. Evers, Phys. Chem. Chem. Phys. **15**, 6684 (2013).
- ³² A. Bagrets, J. Chem. Theory Comput. **9**, 2801 (2013).
- ³³ G. Géranton, C. Seiler, A. Bagrets, L. Venkataraman, and F. Evers, J. Chem. Phys. **139**, 234701 (2013).
- ³⁴ M. Walz, A. Bagrets, and F. Evers, (to be published).
- ³⁵ Methodological details: TURBOMOLE package⁵⁵, DFT with generalized gradient approximation (GGA, BP86 functional)^{56,57} together with a contracted Gaussian-type basis (def2-SVP)⁵⁸ and corresponding Coulomb-fitting basis set within the resolution of the identity (RI) approximation⁵⁹.
- ³⁶ M. Di Ventra, *Electrical Transport in Nanoscale Systems* (Cambridge University Press, 2008).
- ³⁷ F. Evers and A. Arnold, in *CFN Lectures on Functional Nanostructures - Volume 2*, Lecture Notes in Physics, Vol. 820 (Springer Berlin, 2011).
- ³⁸ We calculate the transmission function in a Landauer-Büttiker approach^{60,61}:
- $$T(E) = \text{Tr}(\hat{G} \hat{\Gamma}_L \hat{G}^\dagger \hat{\Gamma}_R), \quad \hat{\Gamma}_\alpha = i(\hat{\Sigma}_\alpha - \hat{\Sigma}_\alpha^\dagger).$$
- Then, the total current is given by
- $$I = \frac{2e}{h} \int_{-\infty}^{\infty} dE (f_L(E) - f_R(E)) T(E)$$
- with $f_\alpha(E)$ being the Fermi functions of the reservoirs.
- ³⁹ M. Y. Han, B. Özyilmaz, Y. Zhang, and P. Kim, Phys. Rev. Lett. **98**, 206805 (2007).
- ⁴⁰ There are two ways to motivate our choice of $L \propto N_C + 1$ (rather than e.g. $L \propto N_C$). First, in order to implement hard-wall BC in a tight-binding model, one would add one further site at each transverse edge with an infinite on-site potential, consequently $L = (N_C + 1)a/2$. Second, a more realistic model would be a box with length $L = (N_C - 1)a/2$ and finite-potential walls with the work function Φ of the nanoribbon as potential height. In this model, the π electrons are located between the two outermost box atoms and the wavefunctions decay outside the box exponentially with the tunneling length scale λ_T . This length scale should approximately coincide with the distance d between the outer carbon atom and the border of the box (see Fig. 1) and is calculated using $\Phi = 4.0 \text{ eV}$ of DFT calculations for ribbons and compared to $a = 2.46 \text{ \AA}$: $\lambda_T = \hbar / \sqrt{2m\Phi} = 0.98 \text{ \AA} \approx a/2$. In the model with infinite-potential walls, d must be chosen in the order of λ_T and $d = a/2$ fulfills this condition.
- ⁴¹ L. Brey and H. A. Fertig, Phys. Rev. B **73**, 235411 (2006).
- ⁴² A. Castro Neto, F. Guinea, N. Peres, K. Novoselov, and A. Geim, Rev. Mod. Phys. **81**, 109 (2009).
- ⁴³ T. Wassmann, A. P. Seitsonen, A. M. Saitta, M. Lazzeri, and F. Mauri, J. Am. Chem. Soc. **132**, 3440 (2010).
- ⁴⁴ Arguments based on wavefunction symmetries and vanishing wavefunction overlap matrix elements have been given that with the adsorption site 1 backscattering is completely suppressed^{9,16}.
- ⁴⁵ H. J. Choi, J. Ihm, S. G. Louie, and M. L. Cohen, Phys. Rev. Lett. **84**, 2917 (2000).
- ⁴⁶ V. Blum, R. Gehrke, F. Hanke, P. Havu, V. Havu, X. Ren, K. Reuter, and M. Scheffler, Comput. Phys. Commun. **180**, 2175 (2009).
- ⁴⁷ J. Tersoff and D. R. Hamann, Phys. Rev. Lett. **50**, 1998 (1983).
- ⁴⁸ E. Clar, *The Aromatic Sextet* (Wiley New York, 1972).
- ⁴⁹ M. Solà, Front. Chem. **1**, 22 (2013).
- ⁵⁰ M. Nakaya, Y. Kuwahara, M. Aono, and T. Nakayama, J. Nanosci. Nanotechnol. **11**, 2829 (2011).
- ⁵¹ N. Bajales, S. Schmaus, T. Miyamashi, W. Wulfhekel, J. Wilhelm, M. Walz, M. Stendel, A. Bagrets, F. Evers, S. Ulas, B. Kern, A. Böttcher, and M. M. Kappes, J. Chem. Phys. **138**, 104703 (2013).
- ⁵² T. Druga, M. Wenderoth, F. Lüpke, and R. G. Ulbrich, Appl. Phys. Lett. **103**, 051601 (2013).
- ⁵³ L. Yan, C. Punckt, I. A. Aksay, W. Mertin, and G. Bacher, Nano Lett. **11**, 3543 (2011).
- ⁵⁴ Y.-J. Yu, Y. Zhao, S. Ryu, L. E. Brus, K. S. Kim, and P. Kim, Nano Lett. **9**, 3430 (2009).
- ⁵⁵ R. Ahlrichs, M. Bär, M. Häser, and C. Kölmel, Chem. Phys. Lett. **162**, 165 (1989).
- ⁵⁶ A. D. Becke, Phys. Rev. A **38**, 3098 (1988).
- ⁵⁷ J. P. Perdew, Phys. Rev. B **33**, 8822 (1986).
- ⁵⁸ A. Schäfer, H. Horn, and R. Ahlrichs, J. Chem. Phys. **97**, 2571 (1992).
- ⁵⁹ K. Eichkorn, F. Weigend, O. Treutler, and R. Ahlrichs, Theor. Chem. Acc. **97**, 119 (1997).
- ⁶⁰ R. Landauer, IBM J. Res. Dev. **1**, 223 (1957).
- ⁶¹ M. Büttiker, Y. Imry, R. Landauer, and S. Pinhas, Phys. Rev. B **31**, 6207 (1985).